



OPEN

Rapid Charging of Thermal Energy Storage Materials through Plasmonic Heating

SUBJECT AREAS:
ORGANIC-INORGANIC
NANOSTRUCTURES
NANOPHOTONICS AND
PLASMONICS

Zhongyong Wang^{1*}, Peng Tao^{1*}, Yang Liu¹, Hao Xu¹, Qinxian Ye¹, Hang Hu¹, Chengyi Song¹, Zhaoping Chen², Wen Shang¹ & Tao Deng¹

Received
24 June 2014

Accepted
11 August 2014

Published
1 September 2014

Correspondence and requests for materials should be addressed to W.S. (shangwen@sjtu.edu.cn) or T.D. (dengtao@sjtu.edu.cn)

* These authors contributed equally to this work.

¹State Key Laboratory of Metal Matrix Composites, School of Materials Science and Engineering, Shanghai Jiao Tong University, Shanghai 200240, P. R. China, ²Research Institute, Baoshan Iron & Steel Co. Ltd, Shanghai 201900, P. R. China.

Direct collection, conversion and storage of solar radiation as thermal energy are crucial to the efficient utilization of renewable solar energy and the reduction of global carbon footprint. This work reports a facile approach for rapid and efficient charging of thermal energy storage materials by the instant and intense photothermal effect of uniformly distributed plasmonic nanoparticles. Upon illumination with both green laser light and sunlight, the prepared plasmonic nanocomposites with volumetric ppm level of filler concentration demonstrated a faster heating rate, a higher heating temperature and a larger heating area than the conventional thermal diffusion based approach. With controlled dispersion, we further demonstrated that the light-to-heat conversion and thermal storage properties of the plasmonic nanocomposites can be fine-tuned by engineering the composition of the nanocomposites.

With the rapid increase of human population and great concern for fuel depletion, the development and utilization of renewable solar energy have been receiving intensive attention. Photothermal conversion, as a direct and efficient technology to harness solar energy, has great advantages such as high achievable efficiency, low cost, and minimized pollution generated from the manufacturing processes^{1,2}. Thermal storage materials have been considered as one of the key components for the efficient and versatile use of the solar energy after photothermal conversion, and to adjust the time discrepancy between power supply and demand^{3–8}. Among various thermal energy storage materials, organic thermal storage materials have shown good features such as high energy storage density, chemical stability, cost effectiveness and non-corrosiveness^{6–8}.

The slow heating rate of the organic thermal storage materials that is associated with their low thermal conductivities, however, has become a severe limitation to their further development and applications. To address this issue, in the past, high thermal conductivity fillers such as metallic particles⁹, metal oxide particles¹⁰, graphite^{11–13}, carbon nanotube/nanofiber^{14–17}, graphene¹⁸ and graphene oxide^{19,20} were incorporated to improve the overall thermal conductivity, and to speed up the heat transfer rate from the solar absorber to the thermal storage materials. As compared to improving thermal conductivity²¹, in recent years increasing attention has been devoted to directly collecting and converting solar radiation to thermal energy^{15,17,22–26}. Previously, Tang et al prepared rapid visible light harvesting thermal storage materials by integrating organic dye molecules into poly(ethylene glycol) matrix to absorb visible light and convert it into heat^{22,23}. Recently, Wang et al compared the photothermal conversion efficiency among gold (Au) nanoparticles (NPs), PbS NPs, organic dyes, and carbon black at the same mass concentration within water solution and found that small size Au NPs had the best performance in terms of conversion efficiency and conversion stabilities²⁷.

In this work, we make use of the photothermal effect of noble metal NPs^{28–32} to speed up the heating rate of organic thermal storage materials. Very low volumetric loading concentration (ppm level) of surface modified Au NPs and nanorods (NRs) were homogeneously dispersed into transparent gel wax matrices. Upon illumination with a green laser, the uniformly distributed Au NPs/NRs can instantly convert optical energy into plasmonic heat at nanometer scale and the converted thermal energy can be immediately transferred to the whole bulk sample, thereby realizing fast heating of the thermal storage matrix materials. We further demonstrate that the plasmonic nanocomposites could directly harvest sunlight and store solar energy, and would have important applications for renewable energy.

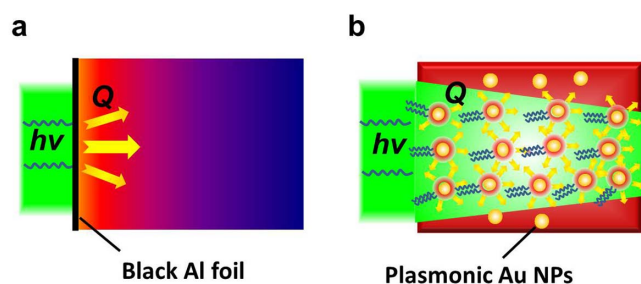


Figure 1 | Schematic illustration of two different charging approaches of thermal storage materials. (a) Conventional thermal diffusion based slow charging, (b) Instant optical charging via plasmonic heating of uniformly dispersed Au NPs.

Results

Fig. 1a presents that conventional thermal charging of organic thermal storage materials relies on the slow thermal heating, mainly through thermal diffusion, from the hot zone, here shown as a black aluminum (Al) foil that absorbs incident light and converts it into heat, to the rest part of thermal storage media. Fig. 1b shows that our new approach utilizes homogeneously dispersed Au NPs, which act as numerous local optical heaters, to continuously heat up the whole organic thermal storage matrix materials. Therefore, the whole bulk thermal storage materials could be immediately and uniformly heated. Instead of using the traditional opaque paraffin wax phase-change material that would strongly scatter the incident visible light, in this work we utilize a transparent gel wax as the model organic sensible thermal storage material (see Fig. S1 in Supplementary Information) to facilitate the excitation of the plasmonic heating of the incorporated Au particles. This facile approach could be easily applied to other thermal storage material systems.

To achieve a homogeneous mixing with the gel wax matrix, spherical Au NPs were synthesized within the non-polar toluene solvent by using oleylamine as the stabilizing agent³³. As shown by the TEM

image and particle size distribution histogram in Fig. 2, nearly mono-disperse Au NPs (with an average diameter of 10.5 ± 1.5 nm) were obtained. Owing to the effective surface protection of the long alkane chain of oleylamine, the synthesized Au NPs can be readily mixed with and dispersed into gel wax, which chemically is a mineral oil made up of alkanes with different chain lengths (C15 to C40) and thickened by styrene butadiene rubber (~ 10 wt%) according to manufacturer's specification (Shanghai Lida Industrial, Co., Ltd). As the loading concentration increases, the pink color of the composite becomes darker, but they still maintain a high optical transparency. UV-Vis spectra in Fig. 2d show the same absorption peak centered at 535 nm and the peak intensity increases linearly with the increasing concentration of the Au NPs. Both the high optical transparency and consistent plasmonic absorption peaks indicate a homogeneous dispersion of Au NPs within the gel wax matrix. Free of aggregation is crucial not only for the successful penetration of the incident light but also the effective excitation of plasmonic NPs.

We first used a green laser (~ 532 nm in wavelength, with a focused beam diameter of 1.5 mm) to excite the Au NPs around their plasmonic resonance wavelength. Fig. 3 shows the experimental setup and time-sequential IR images of the thermal storage materials during the heating process. A neat gel wax and a gel wax sample with black Al foil were used as the control sample and the benchmark, respectively. In the neat gel wax sample, only a weak narrow light path in the center of the cuvette was observed. There was negligible change in the sample temperature because the gel wax could not effectively absorb the green laser radiation. For the gel wax-Al foil sample, as the black Al foil was attached onto the inner side of cuvette where the laser beam entered, the hot zone gradually expanded from that side to the middle. When the illumination time was prolonged to 60 s, about 1/3 area of the gel wax was heated. By contrast, in the Au NPs loaded gel wax samples, an instant and uniform heating zone was observed. Here the heating zone was defined as the high temperature area enveloped by the red contour shown by the IR images under the same temperature scale bar. For the two low loading samples, after 10 s illumination the entire sample length coinciding with

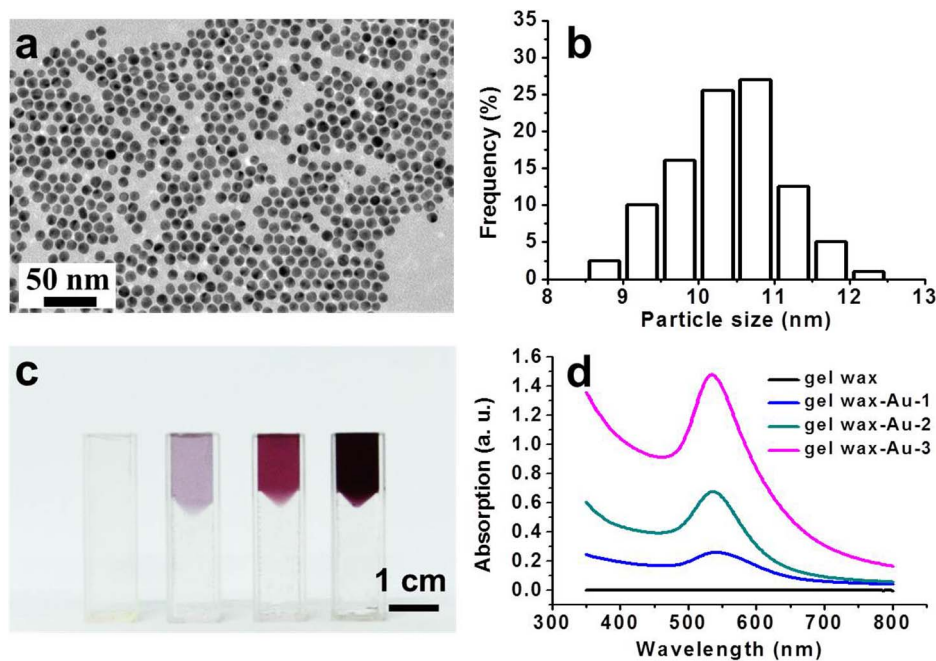


Figure 2 | Synthesis and characterization of Au NP loaded gel wax. (a) TEM image of the synthesized Au NPs; (b) Particle size distribution analyzed by ImageJ; (c) Photograph of neat gel wax and gel wax loaded with increasing loading concentrations of Au NPs from left to right: 6.06×10^{-4} vol% (gel wax-Au NP-1), 1.82×10^{-3} vol% (gel wax-Au NP-2), and 3.64×10^{-3} vol% (gel wax-Au NP-3). (The plasmonic composite was placed on top of transparent neat gel wax. The scale bar is 1 cm.); (d) UV-Vis spectra of neat gel wax and gel wax loaded with Au NPs.

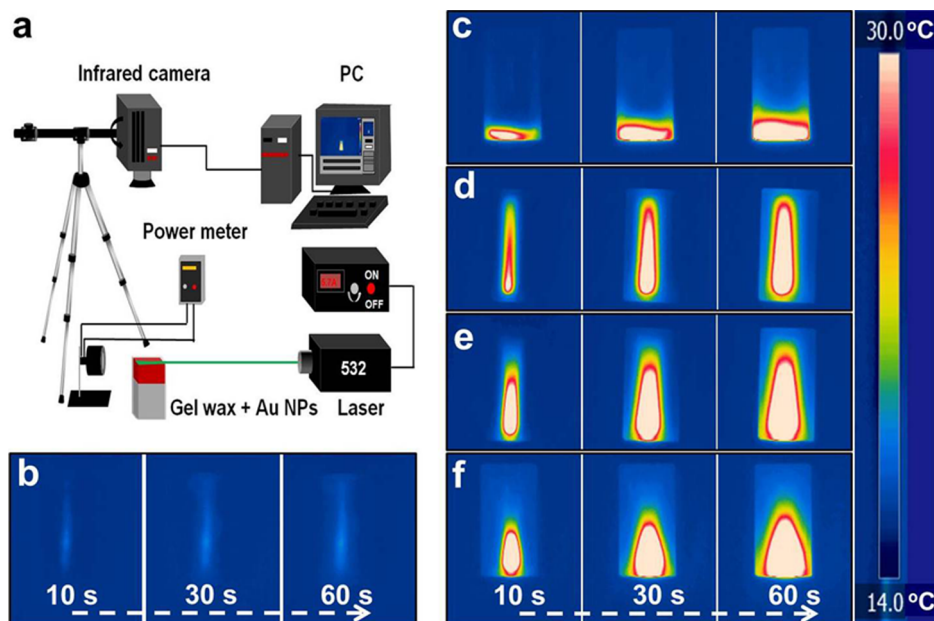


Figure 3 | Schematic of laser illumination experimental setup and time-sequential IR images. (a) A 532-nm green laser with a power density of 36.3 W/cm^2 was used to excite the plasmonic Au NPs and a thermal IR camera was used to capture the temperature change operating at a video mode. The schematic was drawn by Z. W. with Microsoft PowerPoint. Time-sequential IR images obtained from FLIR R&D software: (b) neat gel wax; (c) gel wax-Al foil; (d) gel wax-Au NP-1; (e) gel wax-Au NP-2; (f) gel wax-Au NP-3 after laser illumination of 10, 30 and 60 s. The scale bar is 1 cm.

the laser path was heated up. Prolonging the illumination time to 30 s and 60 s further increased the local temperature and the hot zone became broader. This series of IR images vividly demonstrate that plasmonic heating charging process proceeds via an instant volumetric heat generation in the light absorption region followed by thermal diffusion-limited heat transfer to the remaining portion of the sample. This charging mechanism is in obvious contrast to the thermal diffusion based traditional charging method evidenced by the slow movement of the hot zone from the front (Fig. 3c). When the NP loading concentration became higher, the hot zone slowly enlarged with illumination duration (Fig. 3f). This gradual enlargement could be ascribed to the stronger absorption of the incident light and the shorter optical path at higher loading concentration. The incident light interacted with Au NPs in the front surface and produced a hot zone via plasmonic heating. At the later stage, the plasmonic NPs continuously generated heat and the produced heat is then gradually conducted to the remaining relatively cold gel wax.

The temperature distribution of the thermal storage materials as a function of time was recorded by the IR camera operating at a video mode. Fig. 4 plots the change of the maximum temperature and average temperature over the whole cross area of the sample in the laser heating and natural cooling process after switching off the laser. The neat gel wax sample showed a nearly constant room temperature profile (with a temperature fluctuation of $1\text{--}2^\circ\text{C}$) as the incident laser beam (0.641 W) was detected by the power meter at the back side of the cuvette. The difference between the incident power and measured transmitted power was mainly due to the reflection and scattering loss at the cuvette interfaces. For all other samples, no transmitted light was detected. Upon loading Au NPs, Fig. 4a shows that the maximum temperature profile quickly reached a plateau. Under the same laser illumination, within ~ 1 min the composite samples reached 53°C , 92°C and 160°C from room temperature, respectively. The saturation temperature value increased accordingly with increasing loading concentration of Au NPs. The temperature was determined by the balance among input laser energy, heat absorption and heat dissipation rate of the whole system³⁴. When the energy

input and loss becomes equal, the maximum temperature remains unchanged in the rest of the heating process.

After illuminating for 10 min, the laser was turned off and the sample was left to cool down naturally. Fig. 4b shows that the cooling rate, which was derived from the slope of the maximum temperature profile in the cooling process, continuously decreases and the curves almost overlapped with each other at the low temperature range. It was also observed that the gel wax-Al foil sample shows a larger cooling rate than the gel wax filled with Au NPs at the same temperature range because of the direct contact of the black Al foil with surrounding environment. According to Newton's law of cooling ($\frac{dT}{dt} \propto (T_t - T_a)$), the cooling rate is proportional to the temperature difference between the thermal storage materials (T_t) and the ambient temperature (T_a)³⁵. The higher the temperature at the end of the heating stage, the larger the driving force for cooling. Fig. 4d shows that the average temperature cooling rate did not immediately drop. Instead, it continuously increased, reached a maximum, and then dropped. This phenomenon probably could be related with the fact that the IR camera recorded the surface temperature and the inner hot part compensated the surficial heat loss before reaching the steady heat conduction state. The increasing temperature profile in Fig. 4c also indicates that the average temperature of the tested sample has not reached the steady state.

Fig. 4c shows that all the Au NP filled plasmonic nanocomposite samples have higher temperature values than the conventional thermal diffusion based gel wax-Al foil sample. This difference could be understood from the comparison of IR images in Fig. 3. The Au NP loaded gel wax samples were uniformly heated but the gel wax-Al foil sample was only heated from one side. The far penetration of the incident beam in the Au NPs filled samples was also reflected by their high temperature at the light exit side of the cuvette (see Fig. S4 in Supplementary Information). Assuming the incident laser light was converted into thermal energy, the higher heating temperature and larger heating area imply higher light-to-heat conversion efficiency. This increased efficiency clearly demonstrates the advantage of plasmonic heat charging approach.

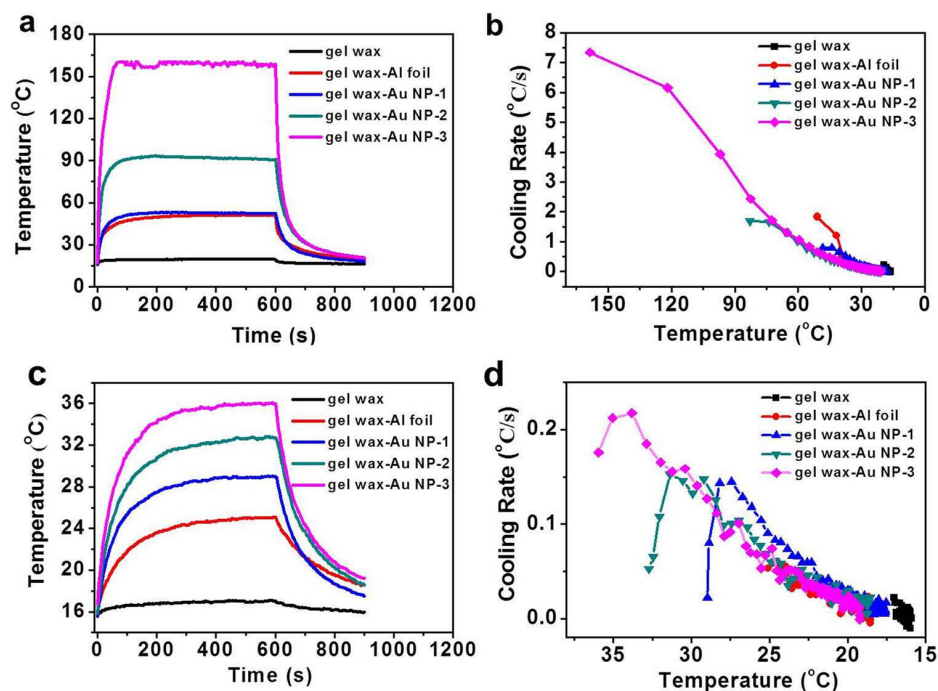


Figure 4 | Temperature profiles of thermal storage materials under laser illumination. (a) Maximum temperature profiles during heating and natural cooling; (b) Cooling rate based on maximum temperature; (c) Average temperature profiles during heating and natural cooling; (d) Cooling rate based on average temperature.

We further demonstrate that the prepared homogeneously dispersed nanocomposites could directly convert renewable solar energy, here provided by a solar simulator (with a power density of 7.2 W/cm^2), and store it as thermal energy. The IR images in Fig. 5 display that the Au NP loaded gel wax samples had a much larger and more uniform hot zone than the samples with Al foil. Different from green laser illumination, the neat gel wax sample was also heated to $\sim 60^\circ\text{C}$ under the broad spectrum sunlight radiation. The IR portion of the sunlight could be effectively absorbed by the gel wax sample leading to the temperature rise. Comparing the gel wax-Al foil sample and nanocomposite samples, the black Al foil can fully absorb the incident sunlight, thus the front portion of the gel wax was immediately heated up. Further increasing the illumination time to 30 s and 60 s, the hot zone only expanded slowly by the intrinsic slow thermal diffusion mechanism. It should be emphasized that the Au NPs are most effectively excited only near their resonant peak ($\sim 530 \text{ nm}$) and the plasmonic nanocomposites only absorb a small portion of the incident sunlight. However, even with such a low loading of Au NPs, they showed much better performance than the benchmark sample.

Figs. 5f and 5g show the average temperature and the temperature at the light exit side of the cuvette during the sunlight heating and natural cooling process. After illumination for 1 min, the temperature of the benchmark gel wax-Al foil sample rose from 17.7°C to 42.8°C , but the temperature of the gel wax with Au NPs increased to 71.2°C for the gel wax-Au NP-3 sample. If assuming all the absorbed solar energy was converted into heating the same amount of sensible thermal storage gel wax, then the amount of heat stored is proportional to the increment of the average temperature since. Such comparison would indicate a more than 75% improvement of photothermal conversion and storage efficiency for the gel wax-Au NP-3 sample over the benchmark gel wax-Al foil sample. Calculation of the slope of temperature curve indicates that the heating rate of the gel wax-Au NP-3 sample ($\sim 0.89^\circ\text{C/s}$) is more than twice of the gel wax-Al foil sample ($\sim 0.42^\circ\text{C/s}$). The temperature profiles at the light exit side of the sample also confirmed the uniform heating advantage in the plasmonic nanocomposite samples.

We also prepared gel wax filled with Au NRs and studied their direct solar conversion and thermal storage properties. The as-synthesized NRs (diameter: $17 \pm 2.2 \text{ nm}$, length: $72 \pm 8.8 \text{ nm}$) were stabilized by hexadecyltrimethylammonium bromide (CTAB) and were able to form a pink aqueous dispersion. To be compatible with the gel wax matrix, the synthetic CTAB ligands were exchanged with a long alkyl chain thiol (dodecanethiol) that can form a strong gold sulfur bond with Au NRs and the alkyl chains can favor the dispersion of NRs within gel wax. Fig. 6a shows that with the same mass concentration both gel wax-Au NP composites and gel wax-Au NR composites are highly transparent. The UV-Vis spectra show that gel wax-Au NR composites have a small transverse plasmonic peak at $\sim 520 \text{ nm}$ and a large broad longitudinal plasmonic peak centered at $\sim 850 \text{ nm}$. Quantitatively, the gel wax-Au NR composites have stronger absorption than the gel wax filled with spherical Au NPs. The difference in plasmonic absorption intensity could be related to the much larger extinction coefficient of the high aspect ratio Au NRs^{36–39}. The calculation work from Coronado et al³⁸ showed that with the same equivalent volume, the extinction coefficient of cylinder-shaped Ag NRs is several times of spherical NPs and this difference became more dramatic with larger individual particle size. Based on the fitting formula reported by Huo et al³⁶, the extinction coefficient of oleylamine-capped Au NPs in the gel wax matrix was estimated to be $\sim 1.21 \times 10^8 \text{ M}^{-1} \text{ cm}^{-1}$ by inputting the diameter (10.5 nm) of our NPs. Similarly, the extinction coefficient of Au NRs in gel wax matrix was estimated to be $\sim 5.25 \times 10^9 \text{ M}^{-1} \text{ cm}^{-1}$ according to its dependence on aspect ratio of NRs³⁷. At the same mass concentration, the NP/NR number ratio is ~ 25 , if we assume the NPs are spheres with a diameter of 10.5 nm, and the NRs are cylinders capped with two hemispheres. With these parameters, we could estimate their absorbance according to the Beer-Lambert law and found that the absorption of the NR sample is ~ 1.75 times of the NP composite sample. This value is close to the absorption peak ratio (~ 1.92) of the peak maximum at $\sim 850 \text{ nm}$ for the gel wax-Au NR-1 sample and the peak maximum at $\sim 520 \text{ nm}$ for the gel wax-Au NP-1 sample.

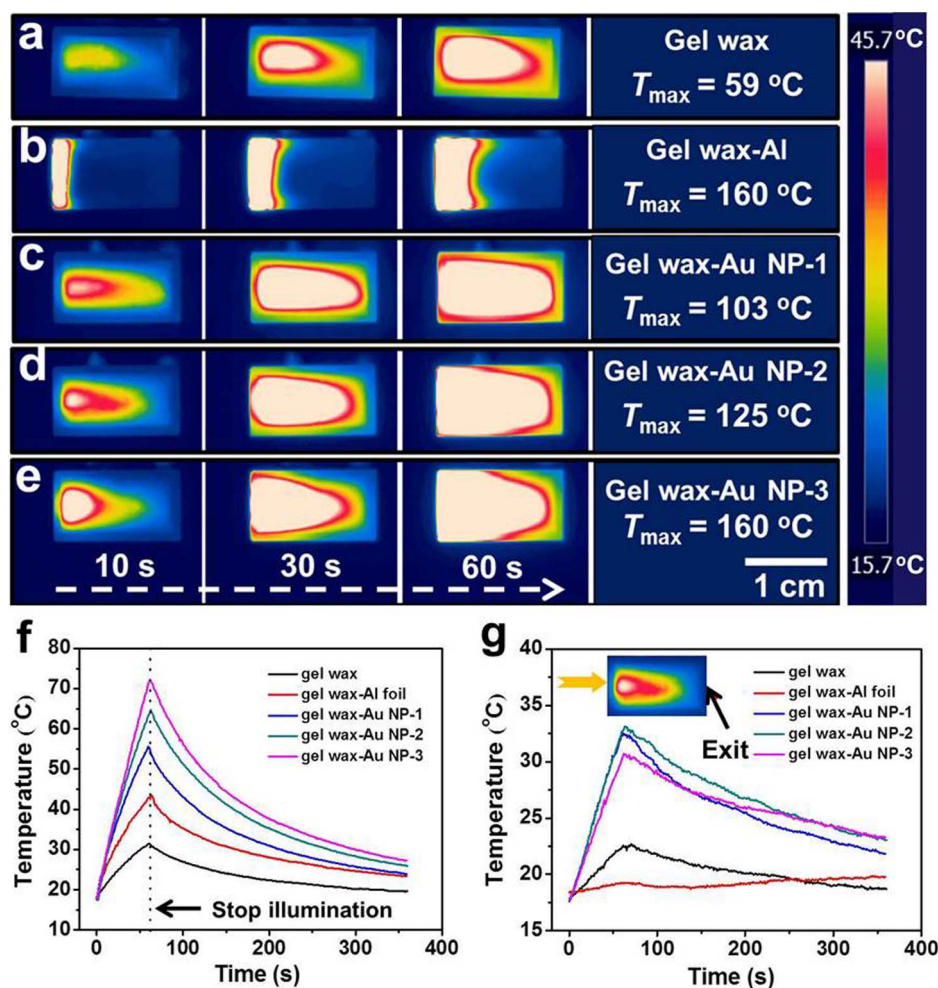


Figure 5 | Time-sequential thermal IR images and temperature profiles of thermal storage materials under solar illumination. IR images of (a) neat gel wax; (b) gel wax-Al foil; (c) gel wax-Au NP-1; (d) gel wax-Au NP-2; (e) gel wax-Au NP-3. (f) Average temperature profile. (g) Temperature profile of thermal storage materials at the light exit side. The inset shows a typical IR image where the temperature value was analyzed as the point in the light exit side of the cuvette.

Gel waxes filled with the same mass concentration of Au NPs and NRs were subjected to sunlight illumination under a decreased power density of 2.9 W/cm^2 , considering the possible reported shape change of Au NRs at high temperatures^{40,41}. With the same homogeneous dispersion within gel wax, the IR images in Fig. 6b present that both nanocomposites have a similar uniform heating area. The average temperature profiles in Fig. 6c indicate that under the same illumination condition the temperature of the gel wax-Au NR-1 sample is 1/3 higher than the gel wax-Au NP-1 sample. The heating and cooling curves of the temperature at the light exit side of the sample in Fig. 6d show that these two curves almost overlapped. The slightly high temperature from the gel wax-Au NP-1 sample is due to the relative weak absorption and further penetration of the incident sunlight. We also mixed Au NPs and NRs together to fine-tune the absorption spectrum of the composites, *i. e.* the relative absorption intensity of different peaks, and tested the photothermal storage properties. By adding NRs into the gel wax-Au NP-1 sample at a NR/NP mass ratio of 0.37 : 1, the resultant nanocomposites have the characteristic peak at $\sim 850 \text{ nm}$ from the added NRs, and its relative intensity is lower than the peak at $\sim 520 \text{ nm}$. With this composition, the mixed NP/NR gel wax nanocomposite sample demonstrated an intermediate average temperature increase under the same solar irradiation, that is higher than the gel wax-Au NP-1 sample, but lower than the gel wax-Au NR-1 sample. (see Fig. S7 in Supplementary Information) Owing to their homogeneous distribution state,

they showed similar temperature profiles at the light exit side of the sample.

Discussion

Unlike the previous efforts in improving thermal conductivity of the organic thermal storage materials, we resort to the fast optical-thermal heating effect of the plasmonic NPs/NRs. In our case, the volumetric ppm level loading concentration is too low to increase the apparent thermal conductivity^{9,10,14,16}. The Au NP/NR surfaces are decorated with organic oleylamine or thiol molecules. This organic layer would also prevent the formation of percolated thermal conductive path. Indeed, thermal conductivity measurement (TPS 2500 Thermal Constants Analyzer, Hot Disk AB, Gothenburg, Sweden) showed that both the neat gel-wax and the gel-wax loaded with Au NPs/NRs have the same thermal conductivity ($\sim 0.2 \text{ W/m}\cdot\text{K}$). Compared with the strategies reported in enhancing thermal conductivity, the loading concentration of Au NPs/NRs is extremely low in our approach. This low loading requirement would also significantly bring down the cost and make this technology to be very attractive for large scale production and applications.

In general, good dispersion of nanofillers within the polymeric matrices is a prerequisite for the nanocomposites to achieve high performance^{42–45}. The effective surface ligand engineering with oleylamine and dodecanethiol successfully prevented particle agglomeration and precipitation during repeated tests. The stability of filler

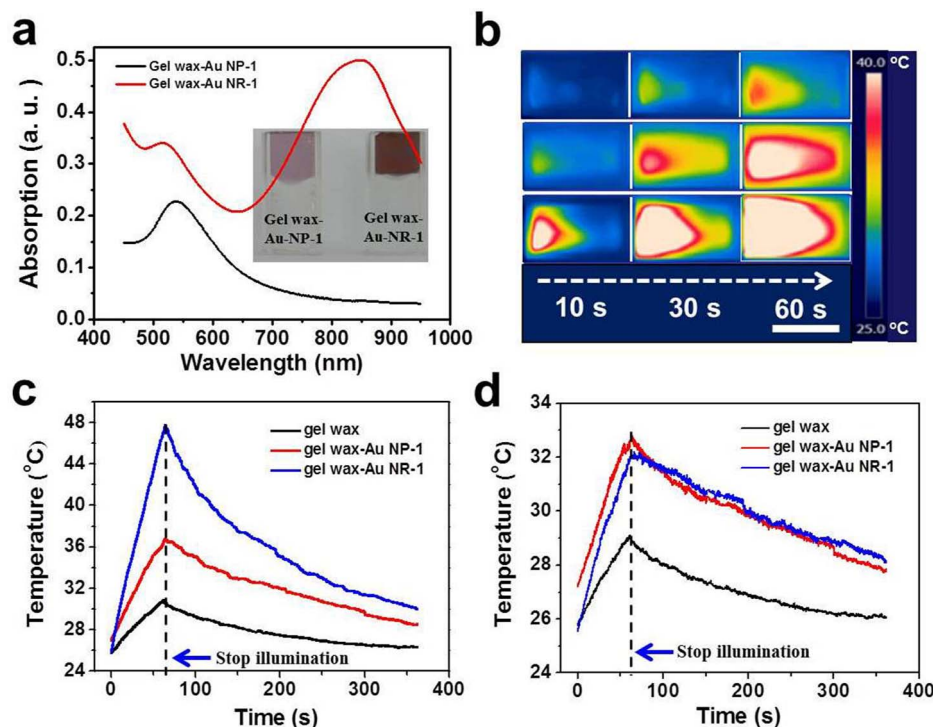


Figure 6 | Comparative thermal storage properties of gel wax filled with Au NPs and Au NRs. (a) UV-Vis absorption spectra of gel wax-Au NP-1 and gel wax-Au NR-1 sample with the same nominal loading concentration. The inset images are the photographs of the prepared composites. (b) Sequential IR image of gel wax, gel wax-Au NP-1 and gel wax-Au NR-1 composite. The scale bar is 1 cm. (c) Average temperature profile during solar illumination and natural cooling. (d) Temperature at the light exit side during solar illumination and natural cooling.

dispersion, in return, ensured consistent performance of the prepared nanocomposites during the repeated heating/cooling test under intense solar illumination (see Fig. S8 in Supplementary Information). The achieved high average temperature of the nanocomposite samples could be attributed to the combined high photothermal conversion efficiency of plasmonic Au particles, which was measured close to 100% upon resonant excitation^{27,28,46}, and the advantageous volumetric heating mechanism. Although the black Al foil has stronger absorption of the sunlight than the plasmonic composites, a large portion of the generated heat at the front surface was lost into the surroundings during its slow transfer process to other parts of the gel wax matrix. In contrast, the heat loss was significantly reduced in the volumetric heating mechanism leading to enhanced thermal storage performance. While previous work showed that smaller size Au NPs have higher photothermal conversion efficiency under laser radiation^{27,46}, in our system, we observed larger temperature increase for the NR filled composites under the broad band solar illumination than the NP filled composites. For one thing, it can be related to the stronger absorption capability of the incorporated Au NRs, particularly the additional absorption of solar light above 700 nm. Another possible benefit from the high aspect ratio NRs is their stronger scattering effect of the incident light. The reabsorption of the scattered light might also contribute to the enhanced photothermal properties²⁷.

In summary, we have demonstrated the fast and uniform heating of organic solar storage materials via plasmonic heat generated by well-dispersed Au NPs/NRs under both laser and solar illumination. Under the same illumination condition, this novel approach leads to a much higher heating rate and temperature than the conventional approach. It was also found that high aspect ratio Au NRs filled nanocomposites have shown better performance than spherical NPs filled composites to collect, convert and store the broad spectrum solar energy as thermal energy. The developed approach could be easily applied to fabricate plasmonic heating charged thermal

storage nanocomposites with different organic matrices, different plasmonic nanofillers, and desired properties based on specific target optical energy sources.

Methods

Synthesis and surface modification of Au NPs. Oleylamine-capped Au spherical NPs were synthesized by modifying the procedure reported by Hiramoto et al.³³. In a typical experiment, 0.1 g of HAuCl₄ (Aladdin Reagent) was added to 40 mL of toluene and sonicated until fully dissolved. Then, 4 mL of oleylamine (Sigma Aldrich) was added. The whole solution was stirred with a magnetic stir bar and refluxed at 120°C for ~1 h. The solution was continuously stirred without heating till it reached room temperature. The synthesized spherical Au NPs were recovered by precipitation with mixed hexane and methanol solvents and high speed centrifugation, and were finally redispersed in toluene to form a transparent dispersion (~1.45 mg/mL).

Synthesis and surface modification of Au NRs. Au NRs were prepared by a seed mediated, CTAB-assisted growth procedure previously reported by Nikoobakht et al.⁴⁷ with some modifications. Seed solution was prepared by adding 0.6 mL of ice-cold 0.01 M NaBH₄ (Aladdin Reagent) to the mixed CTAB solution (5 mL, 0.2 M, Sigma Aldrich) and 5 mL of 0.5 mM HAuCl₄. After stirring for 2 min, the solution was kept at 25°C for 2 h before use. Growth solution was prepared as following. Firstly, CTAB (50 mL, 0.2 M) solution was added to 2.3 mL of 4 mM AgNO₃ solution at 25°C. To this solution, 50 mL of 1 mM HAuCl₄ and 500 µL of 1 M HCl were sequentially added. After gentle mixing, 700 µL of 0.0788 M ascorbic acid was added. Finally, 120 µL seed solution was injected into the growth solution. The resultant mixture was stirred for 30 s and left undisturbed overnight at 30°C for NR growth. The final products were isolated by centrifugation at 8000 rpm for 25 min followed by the removal of the supernatant. The recovered NRs were redispersed in 50 mL deionized water with the aid of ultrasonication.

Au NRs aqueous solution was transferred into chloroform solvent through the following steps^{48,49}. Dodecanethiol (DDT, 50 mL) and acetone (100 mL) were successively added to 50 mL of Au NR solution, and the solution was shaken for 2 min. The solution was thereafter left standing for phase transfer. When the red aqueous layer at the bottom became clear, and the top organic layer turned into red, it indicated the completion of the phase transfer. Methanol (50 mL) was added to the above prepared organic solution to precipitate the NRs. The obtained DDT-capped Au NRs can be easily dispersed in chloroform.

Preparation of nanocomposites. Typically, 10.57 g of paraffin based transparent gel wax (Shanghai Lida Industrial, Co., Ltd) was weighted and melted in a glass vial on a heating stage that was set at 200°C. Subsequently, Au NP dispersion (1 mL, 3 mL and



6 mL) was transferred into the glass vial with a pipette. The whole mixture was stirred overnight to remove toluene. Gel wax–Au NRs nanocomposites were prepared by first melting 4.8 g of gel wax at 98 °C, then mixing with Au NR chloroform dispersion (concentration: 0.985 mg/mL). Considering the low boiling point of chloroform, the prepared composites were subject to a thorough solvent removal process at 98 °C for 3 h. A commercially available and industrially used black aluminum (Al) foil (BKF12, Thorlabs) was used as a bench mark absorber. A rectangle shaped (1 cm × 2 cm × 50 μm) black Al foil was attached to one inner side of the cuvette.

Characterization and measurement of properties. Au NP size and morphology were observed with a TEM (Tecnai G2 Spirit Biotwin, FEI) operating at 120 KV. The particle size distribution was obtained by counting more than 200 particles and analyzing with Image J software (from National Institute of Health, USA). The size and morphology of Au NRs were observed with a high resolution field-emission SEM (FEI, Sirion 200). UV-Vis spectra of neat gel wax and gel wax loaded with Au NPs/NRs were measured by a UV-Vis spectrometer (Lambda 950, PerkinElmer). Light emitted from a 532-nm laser (VA532-3W, Beijing Viasho Technology Co. Ltd) and a solar simulator (94023A, Newport) was used to heat the thermal storage materials. The light emitted from solar simulator was further focused to a spot with a diameter of 1 cm by a PMMA Fresnel lens (size: 28 cm × 28 cm; with a focus length of 31 cm, Shenzhen Salen Technology, Co. Ltd). An infrared (IR) camera (A300S, FLIR Systems Inc) in the video mode was used to capture the sample temperature distribution within the cuvette at a frequency of one hertz. Thermal physical properties of neat gel wax were measured by a differential scan calorimeter (DSC 204F1 Phoenix, Netzsch) with a heating and cooling rate of 5 °C/min.

- Garg, H. P., Mullick, S. C. & Bhargava, A. K. Solar thermal energy storage. (Springer U.S., 1985).
- Badescu, V. Spectrally and angularly selective photothermal and photovoltaic converters under one-sun illumination. *J. Phys. D: Appl. Phys.* **38**, 2166 (2005).
- Liu, C., Li, F., Ma, L. P. & Cheng, H. M. Advanced materials for energy storage. *Adv. Mater.* **22**, E28–E62 (2010).
- Baxter, J. *et al.* Nanoscale design to enable the revolution in renewable energy. *Energy Environ. Sci.* **2**, 559–588 (2009).
- Zhang, Q., Uchaker, E., Candelaria, S. L. & Cao, G. Nanomaterials for energy conversion and storage. *Chem. Soc. Rev.* **42**, 3127–3171 (2013).
- Cabeza, L. F., Sole, C., Castell, A., Oro, E. & Gil, A. Review of solar thermal storage techniques and associated heat transfer technologies. *Proc. IEEE* **100**, 525–538 (2012).
- Cabeza, L. F., Castell, A., Barreneche, C., De Gracia, A. & Fernández, A. I. Materials used as PCM in thermal energy storage in buildings: a review. *Renew. Sust. Energy Rev.* **15**, 1675–1695 (2011).
- Agyenim, F., Hewitt, N., Eames, P. & Smyth, M. A review of materials, heat transfer and phase change problem formulation for latent heat thermal energy storage systems (LHTES). *Renew. Sust. Energy Rev.* **14**, 615–628 (2010).
- Wu, S., Zhu, D., Zhang, X. & Huang, J. Preparation and melting/freezing characteristics of Cu/paraffin nanofluid as phase-change material (PCM). *Energy Fuels* **24**, 1894–1898 (2010).
- Teng, T. P. & Yu, C. C. Characteristics of phase-change materials containing oxide nano-additives for thermal storage. *Nanoscale Res. Lett.* **7**, 1–10 (2012).
- Kim, S. & Drzal, L. T. High latent heat storage and high thermal conductive phase change materials using exfoliated graphite nanoplatelets. *Sol. Energy. Mat. Sol. Cells* **93**, 136–142 (2009).
- Zhong, Y. *et al.* Heat transfer enhancement of paraffin wax using compressed expanded natural graphite for thermal energy storage. *Carbon* **48**, 300–304 (2010).
- Zhang, Z. *et al.* Preparation and thermal energy storage properties of paraffin/expanded graphite composite phase change material. *Appl. Energy* **91**, 426–431 (2012).
- Fan, L. W. *et al.* Effects of various carbon nanofillers on the thermal conductivity and energy storage properties of paraffin-based nanocomposite phase change materials. *Appl. Energy* **110**, 163–172 (2013).
- Wang, Y., Tang, B. & Zhang, S. Single-walled carbon nanotube/phase change material composites: sunlight-driven, reversible, form-stable phase transitions for solar thermal energy storage. *Adv. Funct. Mater.* **23**, 4354–4360 (2013).
- Babaei, H., Kebllinski, P. & Khodadadi, J. M. Improvement in thermal conductivity of paraffin by adding high aspect-ratio carbon-based nano-fillers. *Phys. Lett. A* **377**, 1358–1361 (2013).
- Liu, Z. *et al.* Tailoring carbon nanotube density for modulating electro-to-heat conversion in phase change composites. *Nano Lett.* **13**, 4028–4035 (2013).
- Fang, X. *et al.* Increased thermal conductivity of eicosane-based composite phase change materials in the presence of graphene nanoplatelets. *Energy Fuels* **27**, 4041–4047 (2013).
- Wang, C. *et al.* Graphene oxide stabilized polyethylene glycol for heat storage. *Phys. Chem. Chem. Phys.* **14**, 13233–13238 (2012).
- Zhang, S., Tao, Q., Wang, Z. & Zhang, Z. Controlled heat release of new thermal storage materials: the case of polyethylene glycol intercalated into graphene oxide paper. *J. Mater. Chem.* **22**, 20166–20169 (2012).
- Raam Dheep, G. & Sreekkumar, A. Influence of nanomaterials on properties of latent heat solar thermal energy storage materials—A review. *Energy Conversion and Management*, **83**, 133–148 (2014).
- Wang, Y., Tang, B. & Zhang, S. Novel organic solar thermal energy storage materials: efficient visible light-driven reversible solid–liquid phase transition. *J. Mater. Chem.* **22**, 18145–18150 (2012).
- Wang, Y., Tang, B. & Zhang, S. Visible light-driven organic form-stable phase change materials for solar energy storage. *RSC Adv.* **2**, 5964–5967 (2012).
- Wang, Y., Tang, B. & Zhang, S. Organic, cross-linking, and shape-stabilized solar thermal energy storage materials: A reversible phase transition driven by broadband visible light. *Appl. Energy* **113**, 59–66 (2014).
- Li, Y. *et al.* From biomass to high performance solar–thermal and electric–thermal energy conversion and storage materials. *J. Mater. Chem. A* **2**, 7759–7765 (2014).
- Guo, X. Z. *et al.* Hybrid tandem solar cell for concurrently converting light and heat energy with utilization of full solar spectrum. *J. Power Sources* **195**, 7684–7690 (2010).
- Jiang, R., Cheng, S., Shao, L., Ruan, Q. & Wang, J. Mass-based photothermal comparison among gold nanocrystals, PbS nanocrystals, organic dyes, and carbon black. *J. Phys. Chem. C*, **117**, 8909–8915 (2013).
- Govorov, A. O. & Richardson, H. H. Generating heat with metal nanoparticles. *Nano Today* **2**, 30–38 (2007).
- Jain, P. K., Huang, X., El-Sayed, I. H. & El-Sayed, M. A. Noble metals on the nanoscale: optical and photothermal properties and some applications in imaging, sensing, biology, and medicine. *Acc. Chem. Res.* **41**, 1578–1586 (2008).
- Fang, C., Shao, L., Zhao, Y., Wang, J. & Wu, H. A gold nanocrystal/poly(dimethylsiloxane) composite for plasmonic heating on microfluidic chips. *Adv. Mater.* **24**, 94–98 (2012).
- Wang, Z. *et al.* Bio-inspired evaporation through plasmonic film of nanoparticles at the air–water interface. *Small* DOI: 10.1002/sml.201401071 (2014).
- Neumann, O., Urban, A. S., Day, J., Lal, S., Nordlander, P. & Halas, N. J. Solar vapor generation enabled by nanoparticles. *ACS Nano* **7**, 42–49 (2012).
- Hiramatsu, H. & Osterloh, F. E. A simple large-scale synthesis of nearly monodisperse gold and silver nanoparticles with adjustable sizes and with exchangeable surfactants. *Chem. Mater.* **16**, 2509–2511 (2004).
- Chen, H. *et al.* Understanding the photothermal conversion efficiency of gold nanocrystals. *Small* **6**, 2272–2280 (2010).
- O’Sullivan, C. T. Newton’s law of cooling—a critical assessment. *Am. J. Phys.* **58**, 956–960 (1990).
- Liu, X., Atwater, M., Wang, J. & Huo, Q. Extinction coefficient of gold nanoparticles with different sizes and different capping ligands. *Colloids Surf. B* **58**, 3–7 (2007).
- Orendorff, C. J. & Murphy, C. J. Quantitation of metal content in the silver-assisted growth of gold nanorods. *J. Phys. Chem. B* **110**, 3990–3994 (2006).
- Coronado, E. A., Encina, E. R. & Stefani, F. D. Optical properties of metallic nanoparticles: manipulating light, heat and forces at the nanoscale. *Nanoscale*, **3**, 4042–4059 (2011).
- Garcia, M. A. Surface plasmons in metallic nanoparticles: fundamentals and applications. *J. Phys. D: Appl. Phys.* **44**, 283001 (2011).
- Mohamed, M. B., Ismail, K. Z., Link, S. & El-Sayed, M. A. Thermal reshaping of gold nanorods in micelles. *J. Phys. Chem. B* **102**, 9370–9374 (1998).
- Petrova, H. *et al.* On the temperature stability of gold nanorods: comparison between thermal and ultrafast laser-induced heating. *Phys. Chem. Chem. Phys.* **8**, 814–821 (2006).
- Tao, P. *et al.* TiO₂ nanocomposites with high refractive index and transparency. *J. Mater. Chem.* **21**, 18623–18629 (2011).
- Tao, P., Viswanath, A., Schadler, L. S., Benicewicz, B. C. & Siegel, R. W. Preparation and optical properties of indium tin oxide/epoxy nanocomposites with polyglycidyl methacrylate grafted nanoparticles. *ACS Appl. Mater. Interface* **3**, 3638–3645 (2011).
- Li, Y., Tao, P., Viswanath, A., Benicewicz, B. C. & Schadler, L. S. Bimodal surface ligand engineering: the key to tunable nanocomposites. *Langmuir* **29**, 1211–1220 (2012).
- Tao, P., Li, Y., Siegel, R. W. & Schadler, L. S. Transparent luminescent silicone nanocomposites filled with bimodal PDMS-brush-grafted CdSe quantum dots. *J. Mater. Chem. C* **1**, 86–94 (2013).
- Jiang, K., Smith, D. A. & Pinchuk, A. O. Size-dependent Photothermal conversion efficiencies of plasmonically heated gold nanoparticles. *J. Phys. Chem. C* **117**, 27073–27080 (2013).
- Nikoobakht, B. & El-Sayed, M. A. Preparation and growth mechanism of gold nanorods (NRs) using seed-mediated growth method. *Chem. Mater.* **15**, 1957–1962 (2003).
- Jebb, M., Sudeep, P. K., Pramod, P., Thomas, K. G. & Kamat, P. V. Ruthenium (II) trisbipyridine functionalized gold nanorods. Morphological changes and excited-state interactions. *J. Phys. Chem. B* **111**, 6839–6844 (2007).
- Mahmoud, A. Y., Zhang, J., Ma, D., Izquierdo, R. & Truong, V. V. Thickness dependent efficiency of polymer solar cells with gold nanorods embedded in the photoactive layer. *Sol. Energy. Mat. Sol. Cells* **116**, 1–8 (2013).

Acknowledgments

This work was supported by National Natural Science Foundation of China (Grant No 91333115), Natural Science Foundation of Shanghai (Grant No 13ZR1421500), and the Zhi-Yuan Endowed fund from Shanghai Jiao Tong University. We thank Prof. Han Chen



for using the solar simulator in his lab and Instrumental Analysis Center of Shanghai Jiao Tong University.

Author contributions

W.S. and T.D. conceived the idea and supervised the project. Z.W. and P.T. conducted experiments, wrote the manuscript and made equal contribution to this work. W.S., T.D., Y.L., H.X., Q.Y., H.H., C.S. and Z.C. helped with experimental work and data analysis, reviewed and commented on the manuscript.

Additional information

Supplementary information accompanies this paper at <http://www.nature.com/scientificreports>

Competing financial interests: The authors declare no competing financial interests.

How to cite this article: Wang, Z. *et al.* Rapid Charging of Thermal Energy Storage Materials through Plasmonic Heating. *Sci. Rep.* 4, 6246; DOI:10.1038/srep06246 (2014).



This work is licensed under a Creative Commons Attribution-NonCommercial-NoDerivs 4.0 International License. The images or other third party material in this article are included in the article's Creative Commons license, unless indicated otherwise in the credit line; if the material is not included under the Creative Commons license, users will need to obtain permission from the license holder in order to reproduce the material. To view a copy of this license, visit <http://creativecommons.org/licenses/by-nc-nd/4.0/>